THE JOURNAL OF PHYSICAL CHEMISTRY B

Article

pubs.acs.org/JPCB

On the pH-Responsive, Charge-Selective, Polymer-Brush-Mediated Transport Probed by Traditional and Scanning Fluorescence Correlation Spectroscopy

C. R. Daniels,[†] L. J. Tauzin,[†] E. Foster,[‡] R. C. Advincula,[‡] and C. F. Landes*,[†]

[†]Department of Chemistry, Rice University, Houston, Texas 77251, United States

[‡]Department of Macromolecular Science and Engineering, Case Western Reserve University, Cleveland, Ohio 44106, United States

Supporting Information

ABSTRACT: The complete and reversible charge-selective sequestration of fluorophores by a weak polyelectrolyte brush, poly(2-(dimethylamino)ethylmethacrylate) (PDMAEMA) was demonstrated using fluorescence correlation spectroscopy (FCS). The chemistry and thickness of the weak polyelectrolyte PDMAEMA was tuned reversibly between neutral and cationic polymer forms. Thus, by switching the pH successively, the brush architecture was tuned to selectively trap and release anionic dye probes while continuously excluding cationic molecules. In addition, line-scan FCS was implemented and applied for the first time to a synthetic polymer system and used to identify a new, slower diffusion time on the order of seconds for the sequestered anionic probe under acidic conditions. These results, which quantify the selective sequestration properties of the PDMAEMA brush, are important because they enable a better understanding of transport in polymers and establish a spectroscopic means of evaluating materials with proposed applications in separations science, charge storage/release, and environmental remediation.

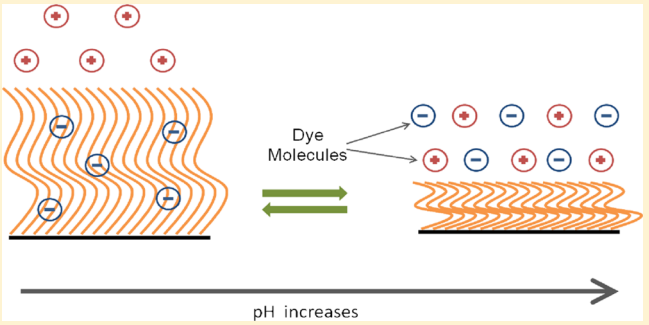

INTRODUCTION

The present work reports on the interaction of cationic rhodamine 6G (R6G) and anionic AlexaFluor 555 (Alexa) dyes with stimuli-responsive polymer brushes, namely, poly(2-(dimethylamino)ethylmethacrylate) (PDMAEMA). Recently, interest in and usage of switchable polymers has increased, with particular emphasis on materials that respond to changes in temperature, pH, and/or ionic concentration.[1−9] Specific applications for switchable polymers include separations science, charge storage/release, and environmental remediation. The weak polyelectrolyte PDMAEMA has the potential to be used in a variety of applications due to its response to pH and temperature.[8,10,11] Already, PDMAEMA has been an integral component for diagnostics and controlled drug delivery applications.[12−14] Therefore, it is important to quantify how PDMAEMA-brush-modified surfaces affect transport of molecular ions as a function of pH, which can directly control thickness, composition, and ionization of the different phases of these polymers.[15,16]

Weak polyelectrolytes have been reported to have more complicated folding and unfolding transitions than the straightforward coil-to-globule model previously embraced due to the mobility of the charges along the weak polyelectrolyte backbone, in contrast to the static charges of strong polyelectrolytes.[17] Many intermediate states may be sampled as the charges move along the backbone, and those states are heavily dependent on pH. Wang and co-workers assessed the local pH around polymer strands in comparison to the bulk pH in polymer-free solutions of FITC.[17] The difference between the local and bulk pH is enlarged with increasing molecular weight (MW) due to the larger number of mobile charges. Thus, it is expected that thicker brush structures would have more complicated pH-dependent structure/function relationships than thinner brushes.

PDMAEMA is a weak polybase. At pHs below the isoelectric point (7.5−8.2), the amine group of the DMAEMA group becomes protonated, as depicted in Figure 1.[18] The Coulombic repulsion that occurs as the protonated groups remain in close proximity on the polymer chain results in an elongation of the chain, resulting in a swelling of the brush layer.[8,10] Conversely, above the isoelectric point, the amine group of the DMAEMA remains uncharged, allowing decreasing interchain repulsion, which in turn results in a dense, collapsed brush.[8,10]

We have successfully used FCS to quantify multiple modes of transport at soft interfaces composed of polymers with static internal structure.[19−23] The benefits of the FCS technique include well-defined focal volumes, low background, and

Special Issue: Paul F. Barbara Memorial Issue

Received: June 1, 2012
Revised: October 18, 2012
Published: October 23, 2012

   dx.doi.org/10.1021/jp3053828 | J. Phys. Chem. B 2013, 117, 4284−4290

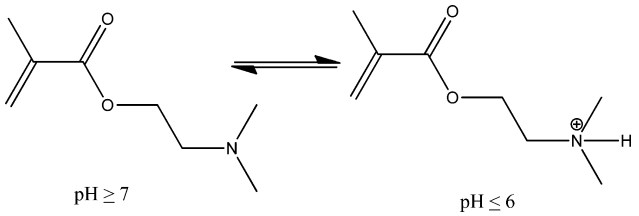

Figure 1. Schematic of the unprotonated (left) and protonated (right) DMAEMA monomer with corresponding pH conditions.

reduction in the probability of photobleaching and photoblinking. However, the tunable structure/function relationship in weak polyelectrolytes raises the potential for transport mechanisms that span many orders of magnitude in the diffusion coefficient. Line-scan FCS is an attractive alternative to traditional FCS and has been developed for understanding slower transport in cellular membranes.[24]

In the present work, we used traditional FCS and line-scan FCS to quantify the presence and extent of interactions between PDMAEMA and both cationic R6G and anionic Alexa dyes. FCS analysis confirmed that the pH-tunable chemistry and structure of the weak PDMAEMA polyelectrolyte resulted in the reversible sequestration and exclusion of the anionic dye, with no interactions observed for the cationic dye. The extent and robustness of switchable and charge-selective sequestration serve as a proof-of-concept demonstration that weak polyelectrolytes could have applications in next-generation separations science materials.

Additionally, line-scan FCS, which is useful for measuring very slow transport, revealed the presence of a new transport component on the order of seconds for the anionic dye interacting with the PDMAEMA system under acidic conditions. To our knowledge, this is the first application of line-scan FCS to synthetic materials, rather than a biological system. These experiments demonstrate conclusively that a homogeneous, tunable surface can selectively and reversibly solvate and release particular solutes, which has broad significance to fields such as sensing, separations, and drug delivery.

METHODS

Materials. Many of the details of the sample preparation, setup, and theory have been previously reported.[19−22,25,26] The 100 nm orange fluorescent carboxylate-modified FluoSphere beads (Invitrogen, max abs/em: 540/560 nm) beads (1:1000 dilution) were used to determine the focal volume for the FCS measurements. Rhodamine 6G (max abs/em: 530/566 nm) and AlexaFluor 555 (max abs/em: 555/565 nm) were diluted to approximately 100 pM for signal versus concentration optimization. KOH (85+%, Sigma-Aldrich) and spectroscopic-grade H_2SO_4 (J. T. Baker) were diluted to 0.001 N solutions, supplying the basic and acidic environments for the fluorescent dyes, respectively. The basic solution was pH 12; the acidic solutions were pH 3 and 5. Hyclone molecular-biology-grade (MB) water (VWR) was used for all dilutions. No. 1 borosilicate coverslips were cleaned using a TL1 wash (80 °C 1:1:6 mixture of NH_4OH/30% H_2O_2/H_2O), followed by oxygen plasma cleaning for 2 min. Measurements were taken in each of the three solutions (aqueous, basic, and acidic) and at a depth of 0.5 μm from the surface.

2-(Dimethylamino)ethylmethacrylate (DMAEMA, 99%) was purchased from Acros Organics. Before polymerization, the inhibitor was removed by passing the compound through a tube containing alternating layers of inhibitor remover and alumina. 1,1,4,7,10,10-Hexamethyl triethylenetetramin (HMTETA, 97%) and copper(I) bromide (CuBr) were purchased from Aldrich and Alfa Aesar, respectively, and used without any modification.

Preparation and Characterization of the PDMAEMA Surface. Self-assembled monolayers of atom-transfer radical polymerization (ATRP)-silane were prepared according to the literature, as depicted in Figure 2.[27] The surface-initiated ATRP

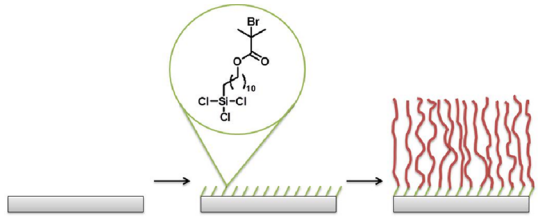

Figure 2. Depiction of the polymerization process.

(SI-ATRP) of PDMAEMA was performed using a typical three Schlenk tube system. The first Schlenk tube contained 5.04 mL of DMAEMA and 40.8 mL of 1,1,4,7,10,10-hexamethyltriethylenetetramine (HMTETA) dissolved in 30 mL of acetone and degassed with N_2 for 30 min. The second and third Schlenk tubes contained 21.6 mg of CuBr and the ATRP-silane monolayer coated slide, respectively. Upon degassing, the contents of tubes 1 and 2 were combined and allowed to stir for 10 min. Then, the solution was transferred to the modified film substrate and allowed to polymerize for the desired time. Three thicknesses of brush were produced, thin, medium, and thick. The thin brush was allowed to polymerize for 6 h, the medium brush was allowed to polymerize for 12 h, and the thick brush was allowed to polymerize for 24 h.

Null ellipsometry was used to determine the thickness of the brush films, as discussed in the Results and Discussion section. All measurements were conducted using a null-ellipsometer operating in polarizer−compensator−sample−analyzer (Multiskop, Optrel Berlin) mode. As a light source, a He−Ne laser (632.8 nm) was applied, and the angle of incidence was set to 60°.

FCS Setup. A solid-state diode laser was the excitation source (VERDI, Coherent). The 532 nm light was circularly polarized, filtered, and expanded to overfill the back aperture of an oil immersion microscope objective (FLUAR 100×, 1.3 NA, Carl Zeiss, GmBH). After excitation, the fluorescence was captured by the same objective[28] and isolated by a dichroic mirror (z532rdc, Chroma Technology) and a notch filter (NHPF-532.0, Kaiser). Fluorescence was then guided through a 50 μm pinhole to block out-of-focus light, increasing the spatial resolution.[29,30] The resulting focal volume had a $1/e^2$ beam radius of ∼270 nm and height of ∼2 μm.[30] Photons were detected by avalanche photodiodes (APD; SPCM-AQR-15, Perkin-Elmer). A piezo stage (P-545.3R2, Physik Instrumente) was controlled using LabVIEW software (National Instruments, 2009) from a DAQ device (NI USB-6229), which allowed the user to maneuver the sample in three dimensions. The output from the APDs was collected by another DAQ device (NI BNC-2121), which was interfaced with a PCI bus (NI-PCI 6602). For each condition, the focal volume was calibrated in order to ensure that no experimental condition altered the confocal beam geometry. It was found that the beam geometry

dx.doi.org/10.1021/jp3053828 | J. Phys. Chem. B 2013, 117, 4284−4290

was consistent throughout the experiments. The theory of FCS is explained in the Supporting Information (SI).

Line-Scan FCS. For line-scan FCS, the focal volume is scanned along a predetermined length continuously, as opposed to the stationary focal volume of traditional FCS. This scanning is performed with a user-defined scan length and time.

In order to calibrate the line-scan method, a 100 nm orange fluorescent carboxylate-modified FluoSpheres bead (Invitrogen, max abs/em: 540/560 nm) adhered to a glass coverslip was scanned. For these measurements, a 2 μm line was scanned repeatedly across the bead. Figure 3 depicts the schematics and

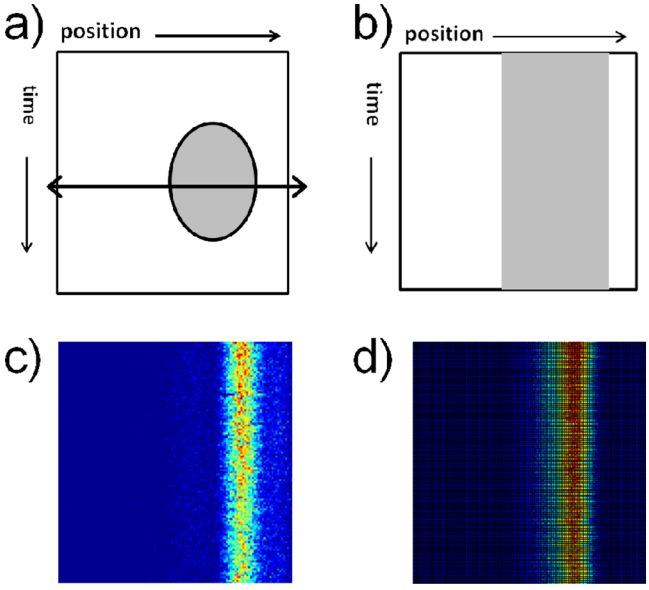

Figure 3. (a) A schematic of a line-scan trajectory across a bead, (b) a schematic of the resultant trace, (c) an image from the slow raster scan program, in which an image is created directly from collected photons, and (d) an image from fast line-scan time trajectories, in which counts versus time are collected and later assembled into an image.

actual images. Figure 3a is a schematic of the program design. The length of the line, the line-scan period, the number of points, and, therefore, the number of lines are all user-defined parameters. The result of this scan should look like that in Figure 3b, where the x-axis is position and the y-axis is time t_i, where t_i is an integer multiple (i) of the scanning period (T_p). Figure 3c is an actual scan from an imaging raster program that is slower than our line-scan program. This program is designed to plot intensities as a function of position, writing out the image, with a user-defined time bin. Such a line-scan imaging process is useful for alignment procedures but is too slow to be useful for performing line-scan FCS.

A faster approach is possible with a line-scan program, which only collects trajectories of intensity as a function of time. This requires an additional program to align the time traces and produce an image. The program corrects for the speed up/slow down velocities that occur at the beginning and end of the line-scans as well as the time needed to return the piezo stage to the starting point. Once calibrated, this results in reproduction of the image depicted in Figure 3d. For both Figure 3c and d, the length of the line, that is, the length of the x-axis, was 2 μm. Because Figure 3c was taken at 128 ms/line, the image is approximately 16 s of data. The faster collection method allowed Figure 3d to be obtained at 26 ms/line, where the image is approximately 3 s of data. Although the line-scan program is an order of magnitude quicker than the raster scanning program, T_p still defines the upper limit of the minimum diffusion time that can be resolved with this method. The minimum diffusion time that the technique can measure is the amount of time that it takes to complete a linear scan, which is limited by the combination of scanning setup and T_p. In this way, line-scan FCS is adequate for measuring slow diffusion.

It is recommended that 10^4–10^5 lines be acquired for this method.[31] For each sample in this study, 10^4 line-scans were acquired. This resulted in a total experiment time of several minutes. The lines were then assembled into a pseudoimage, like that in Figure 3d. Because the vertical axis of the pseudoimage carries time information (Figure 3b), each line (t_i) is a multiple of the scan period (T_p), where $t_i = iT_p$. The autocorrelation is then computed as a function of t_i ($G(0,t_i)$, eq 1) on a logarithmic scale. The choice of a pixel size (s) $\approx r_0$, where r_0 is the focal volume beam radius, leads to a correlation curve that exhibits much less statistical noise than for $s \ll r_0$.[31] The model demonstrated by Ries and Schwille takes into account the finite size of the pixel and was utilized by the authors.[24,31]

$$G(0, \tau_i) = \frac{1}{C\pi s^2}(\sqrt{\pi}\mu_i \operatorname{erf}(\mu_i) + e^{-\mu_i^2} - 1) \quad \text{with} \quad \mu_i = \frac{s}{\sqrt{r_0^2 + 4D\tau_i}} \tag{1}$$

In the current experiment, the dwell time at each pixel was 100 μs. The practical limits on time resolution have been discussed for line-scan[31] and traditional[26] FCS and are taken into consideration for the current work.

For example, traditional FCS can be insensitive to longer-lived events because even though the excitation fluence of our experiments is low, the probability of photobleaching heightens for slower diffusing and adsorbed probes.[32] Line-scan FCS is sensitive to slow diffusion and cannot detect fast diffusion, as shown in Figure 4. For instance, in this experiment, T_p is 26 ms, and therefore, diffusion times faster than 26 ms cannot be detected. This is shown in Figure 4a and b. Figure 4a is a representative line-scan FCS autocorrelation curve resulting from data taken from a 100 nm fluorescent bead sample solvated in 60% sucrose. Theoretically, the characteristic diffusion time for beads in a solution of such high viscosity is 290 ms. From analysis of multiple data sets, we were able to fit the data and found an average characteristic diffusion time of 270 ± 80 ms. In contrast, Figure 4b illustrates that when only fast diffusion is occurring, the line-scan analysis does not extract a diffusion component. The data shown in Figure 4b is a representative line-scan FCS autocorrelation analysis resulting from data taken from a 100 nm fluorescent bead sample solvated in 30% sucrose. Theoretically, the characteristic diffusion time for beads in 30% sucrose solution is 16 ms, irresolvable under the conditions of our line-scan because it is below the resolution of our setup because the diffusion is faster than T_p.

Using FCS to Measure Soft Surface Interactions.[19,25] The fluctuating intensity characterized by FCS arises from the motion of fluorescent molecules as they pass through a tightly focused focal volume, as shown in Figure 5, which depicts our sample and observation volume.[33] Upon calibration, we determined the amount of voltage needed to move the piezo

dx.doi.org/10.1021/jp3053828 | J. Phys. Chem. B 2013, 117, 4284–4290

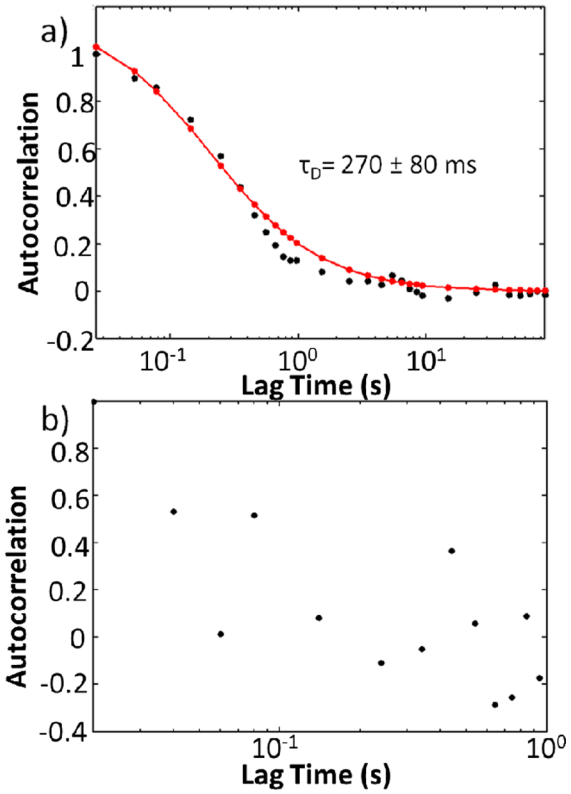

Figure 4. (a) Representative line-scan autocorrelation curve of 100 nm beads in 60% sucrose solution. The theoretical characteristic diffusion time was 290 ms. (b) Representative line-scan autocorrelation curve of 100 nm beads in 30% sucrose solution. The theoretical characteristic diffusion time was 16 ms.

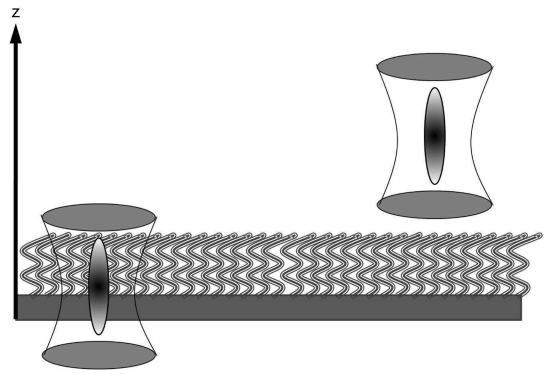

Figure 5. Placement of the polymerized surface with respect to the focal volume. As the focal volume is moved along the *z*-axis, the large observation volume encompasses portions of the polymer and bulk solution. For the present work, the focal volume was positioned either inside of the polymer brush or in the bulk solution. The figure is not drawn to scale.

stage with nanometer precision in *x*, *y*, and *z*. Because we can control the piezo stage axially, measurements can be acquired with the focal volume placed first at the glass surface (Figure 5, far left), corresponding to an offset of 0.5 μm of the beam waist from the glass surface, and at deeper positions within the sample (Figure 5, far right), corresponding to an offset of up to 2.0 μm of the beam waist from the glass surface. In this study, the experiments were performed near the surface, 0.5 μm from the glass surface.

RESULTS AND DISCUSSION

Brush Responds to Changes in pH. Data from the null ellipsometry measurements confirm that PDMAEMA chemistry, and therefore thickness, can be tuned by the pH. This was demonstrated on three different brushes with three different as-synthesized thicknesses. The brush thickness was tuned by changing the pH of the solution used in the measurement. The protonation of the amine group of the monomers, as depicted in Figure 1, results in a Coulombic repulsion along the electrolyte backbone and a swelling of the polymer. This can be seen in Table 1 as the thickness of the brushes at acidic pHs is

Table 1. Ellipsometry Data

Initial Thickness	
thin brush (6 h)	12 ± 2 nm
medium brush (12 h)	38 ± 3 nm
thick brush (24 h)	82 ± 5 nm
pH = 3 Thicknesses	
thin brush	15 ± 1 nm
medium brush	50 ± 2 nm
thick brush	108 ± 5 nm
pH = 12 Thicknesses	
thin brush	10.2 ± 0.3 nm
medium brush	26 ± 3 nm
thick brush	62 ± 2 nm

greater than that of the initial thickness. For instance, the medium brush increases from an initial thickness of 38 ± 3 nm to a thickness of 50 ± 2 nm in a solution at pH 3.This provides evidence that the brush structure can be tuned by controlling the pH.

However, a reduction of hydronium ions also affects the brush as the loss of Coulombic strain results in collapse of the polymer strands. This can also be seen in Table 1 as the thickness of the brushes at basic pHs is lower than that of the initial thickness. For instance, the medium brush decreases from an initial thickness of 38 ± 3 nm to a thickness of 26 ± 3 nm in a solution at pH 12. Thus, the brush structure can be tuned according to pH. In the ensuing experiments, we compare transport of molecular ions within the polymer brush while tuning the chemistry and brush length. In acidic conditions, the monomer side-chain amine groups become protonated. These brushes will have larger spacing between the polymer strands. In basic conditions, the polymer strands collapse and result in thinner, dense structures.

Diffusion Changes as a Function of Electrostatics and Sterics. The change in brush structure as a function of pH allows for steric and electrostatic tunability. As a result of these variables, the next question to address is whether the adaptable brush length and/or the Coulombics involved in the protonation/deprotonation of the monomer side chain influence the transport of molecular probes.

Figure 6 depicts the diffusion times as a function of pH for both cationic and anionic dye probes as measured using traditional FCS with the focal volume positioned within the brush. The experiment included successive switching of the solution pH (between 5 and 12) over the same brush. It is important to confirm that the dye photochemistry is not affected by changes in environment.[34] This was achieved in two ways. First, single-event analysis shows that the average photon counts were not dramatically altered under different solution pH values, demonstrating that the relative quantum yield was

dx.doi.org/10.1021/jp3053828 | J. Phys. Chem. B 2013, 117, 4284−4290

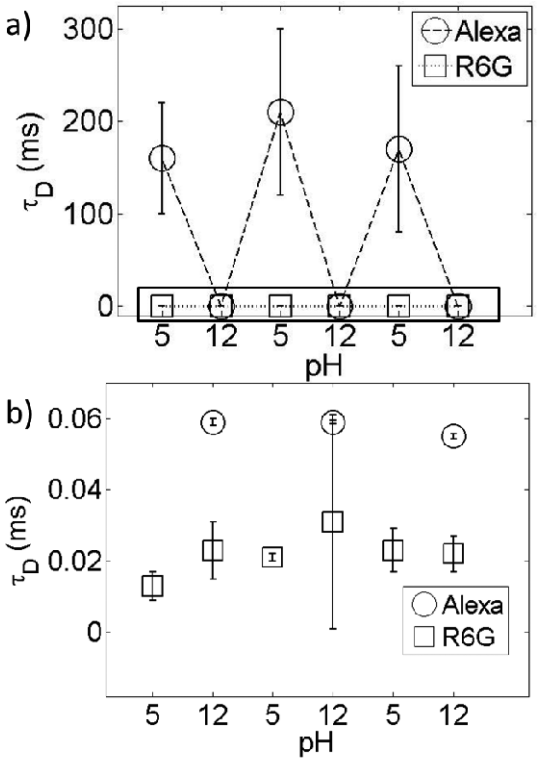

Figure 6. (a) Plot of diffusion times as a function of pH near the surface of the medium brush. These were acquired with traditional FCS as we switched the pH of the solution over the same polymer brush sample. Both the cationic (square marker) and the anionic (circle marker) probes are featured. The cationic probe shows no evidence of interaction at either pH. The anionic probe heavily interacts at pH 3. The anionic probe shows no evidence of interaction at pH 12. Lines are used as guides for the eye. (b) Zoomed-in view of data encased in the black rectangle.

unchanged (Figure S1, SI). Also, in the current and previous research on the current dye systems under similar pH values, we showed that these solution conditions have minimal effect on the extracted diffusive characteristics in comparison to the orders-of-magnitude larger effects due to the charged and crowded environment of the brush (Table S1, SI).[25] This is further demonstrated by the R6G data in Figure 6. Thus, the switchable diffusion characteristics of the Alexa dye can only be attributed to changes due to physical or electrostatic interactions with the switchable brush. This plot shows that the switching of the pH of the brush solution affects only the anionic probe diffusion but does not affect the cationic probe diffusion.

At high pH (12), the measured diffusion times for both dyes were comparable to those of the probes in bulk solution;[25] the diffusion times for the cationic and anionic dyes were 38 ± 5 and 45 ± 3 μs, respectively, at basic pH. It is evident that at the basic pH, when the brush is in its collapsed state, the brush did not garner interaction of the probes. We recently explored the construction of molecular sieves using polymer brushes and reported that pore size can greatly influence the inclusion and exclusion of probes from the brush,[19] resulting in a molecular sieve.[35] The high-pH data shown in Figure 6 are consistent with the earlier studies and suggest that the denser collapsed brush excludes the probes.

At low pH, the cationic probe did not exhibit interaction with the brush. The diffusion time for the positively charged probe at this condition remained comparable to that of the probe in bulk solution;[25] the diffusion time of the cationic probe was 43 ± 3 μs. At low pH (5), the cationic probe is likely excluded from the brush in favor of the hydronium ions present in the solution. However, under the same low-pH conditions, the anionic probe exhibited strong interaction with the brush. The diffusion times were much longer than those of the probes in bulk solution, at least 160 ± 60 ms. The diffusion of the anionic probe in the acidic environment was several orders of magnitude slower than the anionic probe in the basic environment and the cationic probe in both environments. The Coulombic interaction between the anionic probe and the protonated brush is evident in this analysis. There was a large spread in the data for the anionic probe at the low pH. Large standard deviations in FCS data suggest the presence of anomalous or long-lived and unresolved slow events such as aggregation or adsorption.[36] Adsorption events would be expected with a strong Coulombic attraction between the probe and brush. As discussed later, line-scan FCS was used to quantify slow transport.

The data shown in Figure 6 demonstrate that not only can the brush chemistry and structure be tuned to selectively trap and release charged molecules but also that these conditions are reversible and, moreover, that the switchable brush is durable for prolonged periods of time. We alternated the acidic and basic solutions three times, in succession, and observed reproducible results. The preparation and data collection time for a single pH required at least 40 min. The complete time for three cycles of collection was about 4 h. Other experiments (data not shown) demonstrated that the pH-switchable dye anionic interaction was reproducible on the same brush after multiple uses over periods of days and weeks.

Diffusion Changes as a Function of Brush Length. Shown in Figure 7 are the Alexa diffusion times in acidic solutions as a function of ellipsometric thickness, a measure of the steric tunability of the brush. The data in Figure 7 were obtained by traditional FCS. The thin (15 nm), medium (50 nm), and thick (108 nm) brushes were all compared. Figures 7 shows that as the ellipsometric thickness of the polymer brush increases, the diffusion time of the probe decreases. Because of the surface-grafting polymer growth technique, the distance between the polymer strands may be much smaller than the radius of gyration, and this effect increases with increased

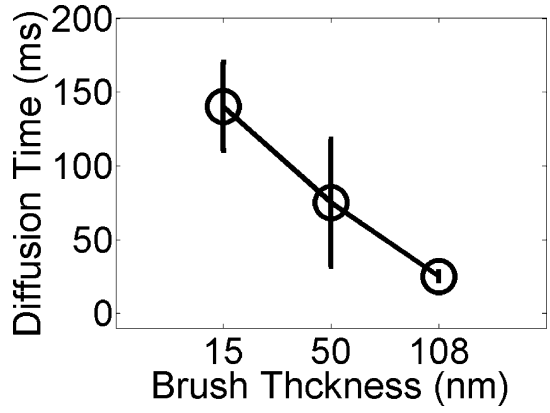

Figure 7. Plot of diffusion times of anionic dye as a function of brush thickness solvated in an acidic solution, acquired with traditional FCS. Lines are used as guides for the eye.

dx.doi.org/10.1021/jp3053828 | J. Phys. Chem. B 2013, 117, 4284−4290

polymer length.[37] We hypothesize that the increase in brush density results in relative reduction of spacing and pore size for longer brushes, which would exclude the dye and result in overall faster detected diffusion because there is relatively more bulk-type diffusion. The FCS experiment shows that although there are relatively small changes in the diffusion of the anionic probe in the acidic environment as the sterics of the brush change, said change is small when compared to the overall trends observed when monitoring the anionic probe in the brush as a function of pH or electrostatics.

It is important to point out that the spread in extracted diffusion times shown in Figures 6 and 7 for Alexa/PDMAEMA under acidic conditions indicates the possibility of even slower processes. Traditional FCS is an inadequate technique to monitor slow dynamics of dye probes because adsorbed or trapped dyes positioned in a stationary focal volume would increase the probability of photoblinking and photobleaching. Also, it has been found that in order to determine accurate diffusion times from traditional FCS autocorrelation curves, the maximum lag must be 5000 times larger than the expected diffusion time.[26] The maximum lag time is the length of the experiment, which means that to accurately determine a characteristic diffusion time on the scale of seconds, we must collect hours worth of data, which exceeds computational and hardware resources. In order to address both of these issues, we designed and applied a line-scan FCS method for the first time to identify slow transport, on the order of seconds, in a synthetic polymer membrane.

Line-Scan FCS Reveals Extremely Slow Diffusion. The line-scan FCS experiments reveal a new slow diffusion component of approximately 14 s for the Alexa/PDMAEMA system under acidic conditions. The values for all systems studied are included in Table 2. Because there was no slow diffusion observed for R6G, as controls, we used 100 nm orange fluorescent carboxylate-modified FluoSpheres beads (Invitrogen, max abs/em: 540/560 nm) in mixtures of water and sucrose with tunable diffusion times. The bead controls show that, as expected, when transport is faster than 26 ms, line-scan FCS cannot detect a diffusion component, such as when beads in 30% sucrose solution were analyzed. When the transport is shifted to the hundreds of milliseconds time scale, as with beads in 60% sucrose, the line-scan FCS autocorrelation analysis allows us to accurately extract the correct diffusion time. The line-scan FCS experiments demonstrate that when the PDMAEMA is swollen and positively charged, an additional extremely slow transport mechanism is active.

Table 2. Slow Component Detected

sample	extracted τ_D (s)
Alexa in thin brush, pH 5	14 ± 1
Alexa in medium brush, pH 5	14 ± 2
Alexa in thick brush, pH 5	13 ± 3
beads in 60% sucrose solution; expected τ_D: 0.29	0.27 ± 0.08
beads in 30% sucrose solution; expected τ_D: 0.016	not detected

Unlike the transport detected by FCS occurring in the ~100 ms time frame, there was no obvious trend in the value of the ~14 s component as a function of polymer thickness, as shown in Table 2. Therefore, we cannot, as was discussed for the ~100 ms component, attribute this component to the relationship between polymer length and polymer density. There are two additional explanations for this slow component. The first is that this component is due to the adsorption/desorption equilibrium between the anionic Alexa dye and local cationic traps within the PDMAEMA, as has been reported for faster processes using other methods.[38] An alternate explanation involves trapping of dyes in brush surface irregularities, which also would not depend on brush thickness. To distinguish the likely mechanism at the current time would require the development and optimization of both complex simulations and alternate polymer synthesis techniques, both of which are outside of the scope of the current work, which focuses both on verifying the tunable internal chemistry of weak polyelectrolyte brushes and the identification of a new diffusion time scale on the order of seconds for Alexa interacting with PDMAEMA in acidic conditions.

CONCLUSIONS

In the present work, we quantified the transport of molecular ions interacting with a weak polyelectrolyte brush. The brush, PDMAEMA, exhibits tunable thickness and chemistry via its reversible transition between a neutral and cationic polymer, as a function of solution pH. Traditional and line-scan FCS techniques were used to probe the dynamics of the interaction of cationic and anionic dyes in acidic and basic conditions. Traditional FCS reveals selective sequestration of an anionic probe within the brush in the acidic environment, whereas no interaction of the cationic probe with the brush was observed. Importantly, the selective sequestration of the anionic probe was complete and reversible, suggesting that these weak polyelectrolyte materials might have uses in separations applications. Line-scan FCS was applied for the first time to a synthetic membrane, and the studies revealed a very strong interaction of the anionic probe with the brush via an additional diffusion time at least 2 orders of magnitude larger than the interaction measure with traditional FCS.

ASSOCIATED CONTENT

Supporting Information

Additional information is available as noted in text. This material is available free of charge via the Internet at http://pubs.acs.org.

AUTHOR INFORMATION

Corresponding Author

*E-mail: cflandes@rice.edu.

Notes

The authors declare no competing financial interest.

ACKNOWLEDGMENTS

C.F.L. thanks the Norman Hackerman Welch Young Investigator Program at Rice University. Additional support for this work was provided by the National Science Foundation (Grants CBET-0854979, DMR 106776, CBET-1134417, and CHE-1151647) and the National Institutes of Health (Grant GM94246-01A1). Acknowledgment is also made to the Donors of the American Chemical Society Petroleum Research Fund for partial support of this research.

REFERENCES

(1) Bashir, R.; Hilt, J. Z.; Elibol, O.; Gupta, A.; Peppas, N. A. *Appl. Phys. Lett.* **2002**, *81*, 3091−3093.

(2) Kanekiyo, Y.; Ono, Y.; Inoue, K.; Sano, M.; Shinkai, S. *J. Chem. Soc., Perkin Trans. 2* **1999**, 557−562.

(3) Lochhead, R.; Padman, V.; Anderson, L.; Wilgus, L. A.; McDaniel, P.; LaBeaud, L.; Davis, K.; Hoff, E.; Epler, J. *Household Pers. Prod. Ind.* **2010**, *47*, 71−76.
(4) Lochhead, R. Y. *ACS Symp. Ser.* **2010**, *1053*, 3−22.
(5) Peteu, S. F.; Oancea, F.; Sicuia, O. A.; Constantinescu, F.; Diinu, S. *Polymers (Basel, Switz.)* **2010**, *2*, 229−251.
(6) Tokarev, I.; Minko, S. *Soft Matter* **2009**, *5*, 511−524.
(7) Tokarev, I.; Motornov, M.; Minko, S. *J. Mater. Chem.* **2009**, *19*, 6932−6948.
(8) Tokarev, I.; Tokareva, I.; Minko, S. *ACS Appl. Mater. Interfaces* **2011**, *3*, 143−146.
(9) Mignet, N.; Richard, C.; Seguin, J.; Largeau, C.; Bessodes, M.; Scherman, D. *Int. J. Pharm.* **2008**, *361*, 194−201.
(10) Jia, H.; Wildes, A.; Titmuss, S. *Macromolecules* **2012**, *45*, 305−312.
(11) Butun, V.; Armes, S. P.; Billingham, N. C. *Polymer* **2001**, *42*, 5993−6008.
(12) Layman, J. M.; Hirani, A. A.; Hunley, M. T.; Lee, Y. W.; Lepene, B.; Thatcher, C. D.; Long, T. E. *PMSE Prepr.* **2007**, *96*, 325−326.
(13) Luo, Y.; Yao, X.; Yuan, J.; Ding, T.; Gao, Q. *Colloids Surf., B* **2009**, *68*, 218−224.
(14) Robbens, J.; Vanparys, C.; Nobels, I.; Blust, R.; Van, H. K.; Janssen, C.; De, S. K.; Roland, K.; Blanchard, G.; Silvestre, F.; et al. *Toxicology* **2010**, *269*, 170−181.
(15) Shiratori, S. S.; Rubner, M. F. *Macromolecules* **2000**, *33*, 4213−4219.
(16) Yoo, D.; Shiratori, S. S.; Rubner, M. F. *Macromolecules* **1998**, *31*, 4309−4318.
(17) Wang, S.; Zhu, Y. *Soft Matter* **2011**, *7*, 7410−7415.
(18) Reis, B. M.; Armes, S. P.; Fujii, S.; Biggs, S. *Colloids Surf., A* **2010**, *353*, 210−215.
(19) Daniels, C. R.; Reznik, C. G.; Landes, C. F. *Colloids Surf., B* **2011**, *88*, 33−38.
(20) Reznik, C.; Berg, R.; Foster, E.; Advincula, R.; Landes, C. F. *J. Phys. Chem. Lett.* **2011**, *2*, 592−598.
(21) Reznik, C.; Darugar, Q.; Wheat, A.; Fulghum, T.; Advincula, R. C.; Landes, C. F. *J. Phys. Chem. B* **2008**, *112*, 10890−10897.
(22) Reznik, C.; Estillore, N.; Advincula, R. C.; Landes, C. F. *J. Phys. Chem. B* **2009**, *113*, 14611−14618.
(23) Daniels, C. R.; Kisley, L.; Kim, H.; Chen, W. H.; Poongavanam, M. V.; Reznik, C.; Kourentzi, K.; Willson, R. C.; Landes, C. F. *J. Mol. Recognit.* **2012**, *25*, 435−442.
(24) Ries, J.; Schwille, P. *Biophys. J.* **2006**, *91*, 1915−1924.
(25) Daniels, C. R.; Reznik, C.; Landes, C. F. *Langmuir* **2010**, *26*, 4807−4812.
(26) Tcherniak, A.; Reznik, C.; Link, S.; Landes, C. F. *Anal. Chem.* **2009**, *81*, 746−754.
(27) Yu, K.; Wang, H.; Xue, L.; Han, Y. *Langmuir* **2007**, *23*, 1443−1452.
(28) Koppel, D. E.; Axelrod, D.; Schlessinger, J.; Elson, E. L.; Webb, W. W. *Biophys. J.* **1976**, *16*, 1315−1329.
(29) Hess, S. T.; Webb, W. W. *Biophys. J.* **2002**, *83*, 2300−2317.
(30) Qian, H.; Elson, E. L. *Appl. Opt.* **1991**, *30*, 1185−1195.
(31) Ries, J.; Chiantia, S.; Schwille, P. *Biophys. J.* **2009**, *96*, 1999−2008.
(32) Petrasek, Z.; Schwille, P. *Biophys. J.* **2008**, *94*, 1437−1448.
(33) Haustein, E.; Schwille, P. *Annu. Rev. Biophys. Biomol. Struct.* **2007**, *36*, 151−169.
(34) Onda, S.; Kobayashi, H.; Hatano, T.; Furumaki, S.; Habuchi, S.; Vacha, M. *J. Phys. Chem. Lett.* **2011**, *2*, 2827−2831.
(35) Schlapak, R.; Caruana, D.; Armitage, D.; Howorka, S. *Soft Matter* **2009**, *5*, 4104−4112.
(36) Schuster, J.; Cichos, F.; Wrachtrup, J.; von Borczyskowski, C. *Single Mol.* **2000**, *1*, 299−305.
(37) Advincula, R. C. *J. Dispersion Sci. Technol.* **2003**, *24*, 343−361.
(38) Wirth, M. J.; Swinton, D. J. *Appl. Spectrosc.* **2001**, *55*, 1013−1017.